Rotating hexagonal pattern in a dielectric barrier discharge system

A. L. Zanin, E. L. Gurevich,* A. S. Moskalenko, H. U. Bödeker, and H.-G. Purwins
Institut für Angewandte Physik, Corrensstr. 2/4, D-48149 Münster, Germany
(Received 14 March 2004; published 13 September 2004)

Here, we report on the experimental observation of a rotating hexagonal pattern in a continuous dissipative medium. The system under investigation is a planar dielectric barrier gas-discharge cell. The pattern consists of a set of current filaments occupying the whole discharge area and rotating as a rigid body. The symmetry of the rotating hexagons is lower than the symmetry of the stationary hexagonal pattern. We study the dynamics of the pattern, especially peculiarities of its rotational velocity. The temperature of the gas is found to be an important quantity influencing the rotating hexagons.

DOI: 10.1103/PhysRevE.70.036202 PACS number(s): 47.54.+r, 52.80.Pi

I. INTRODUCTION

Spatially extended systems being driven far from equilibrium exhibit a large variety of self-organized spatial structures (for an overview see, e.g., [1]). Propagating fronts, waves, solitary structures, spirals, and Turing patterns have been observed and studied. The understanding of properties of the structures is important for the practical use of pattern formation. Important examples for practical implementations are the usage of propagating fronts in semiconductors, which are the basis for the operation of fast switching power thyristors [2], neuronal networks based on thyristor structures [3,4], and Gunn diodes [5] used in high-frequency electronics. Nanodots heterostructures [6,7] represent another example of pattern formation phenomena being promising for use in optoelectronics. Knowledge of pattern formation in granular media [8] is applied for particle segregation in the chemical and food industries [9,10]. Moreover, it is believed that systems capable of self-organization can be potentially applied for information processing (see, e.g., [11]). Data storage algorithms and motion detectors based on photorefractive crystals [12–14] have been developed recently. The understanding of pattern formation is also of crucial importance in medicine [15–17] and biology [18].

From another point of view, even if pattern formation is an undesired effect, the knowledge of its underlying physical nature helps to suppress it. For example, the investigation of pattern formation processes occurring in semiconductor gas-discharge devices used for the conversion of infrared images into the visible has led to the improvement of the technical characteristics of the device [19]. Another example is the successful suppression of undesired patterns occurring by abrasive waterjet cutting [20]. Finally, we want to mention works on control of the traffic flow. It is very important there to reduce the number of self-organized traffic jams [21].

A common type of stationary patterns appearing in nonlinear dissipative media are structures featuring hexagonal symmetry, which have been experimentally and theoretically investigated in hydrodynamical [22], biological and chemical systems [23–25], as well as in granular media [8,26] and dusty plasmas [27,28]. This type of pattern can also be observed in dc- [29,30] and in ac-driven planar gas-discharge systems [31]. The hexagonal patterns in the cited works exhibit no directed collective motion, except for the hexagonal Coulomb crystals in dusty plasmas [27,28], although the onset of rotation should be generic for systems invariant with respect to angular shifts.

To our knowledge, rotation of limited hexagonal clusters has been investigated experimentally and theoretically only for two-dimensional (2D) clusters in dusty plasmas [28]. The motion of the pattern in our experiments is similar to the motion of particles in a Coulomb crystals in dusty plasmas [27,28]. Moreover, in some experiments in helium at voltages lower than the voltage corresponding to the rotating hexagons, we observed intershell rotational motion, similar to [27].

In this paper, we report on the observation of a rotating hexagonal pattern in an ac gas-discharge system, and study its dynamics and symmetry properties. The article is organized as follows. Section II describes the experimental setup and the influence of the cell temperature on the pattern. Section III gives a basic overview on the experimental observation of the rotating hexagonal patterns, its regions of existence as well as the analysis of rotation and deformation of the pattern. The article closes with a conclusion.

II. EXPERIMENTAL SETUP

A. Gas-discharge cell

The experimental system under investigation is schematically shown in Fig. 1. It consists of a gas-discharge cell placed in a vacuum chamber, a high-voltage ac power supply and an image acquisition system connected to a personal computer. The discharge cell has a sandwichlike structure that is comprised of two thin plane-parallel glass plates separated by a thin gas layer. The thickness of the glass plates is $a=0.5$ mm. The gas layer formed by a spacer is $d=0.5$ mm thick and 40 mm in diameter. In order to investigate the pattern formation on domains of different size, a spacer with four separated circular discharge regions having diameters 20, 15, 10, and 6 mm has been used.

*Corresponding author; electronic address: gurevich@uni-muenster.de

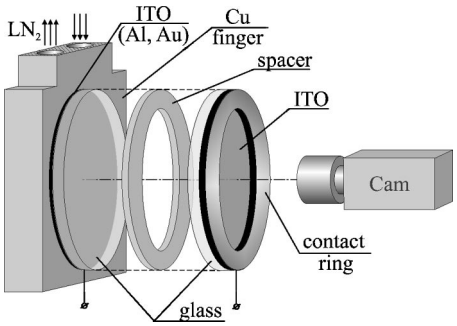

FIG. 1. Schematic representation of the discharge cell. The cell contains transparent ITO electrodes, deposited on glass plates, and a spacer, which, together with the glass plates, forms the discharge area. The discharge is observed with a camera. The spacer contacts both glass plates. The front glass plate is shifted on the scheme to the right and the back glass plate is shifted to the left in order to show the discharge area. The back glass plate is in contact with a cooling system.

The outer sides of the glass plates are coated with indium tin oxide (ITO) electrode layers, which are conductive and transparent to visible light. The system is driven by sinusoidal ac voltage with a frequency of $f=200$ kHz and a voltage amplitude $\hat{U}$ up to 1000 V. When the voltage applied to the system is raised above the breakdown voltage, the gas discharge ignites and various spatial patterns of luminance can be observed.

Principally, patterns can be generated by inhomogeneities occurring in the system, i.e., mainly by improper glass electrodes. To prove spatial homogeneity, we ignite the discharge in a parameter region where no pattern formation is observed and the discharge should be spatially homogeneous. In this way, inhomogeneities being relevant for the present work can easily be identified by differences in local luminance. The measured deviation of the luminance over the whole discharge area does not exceed 10%.

To get an overview of the possible pattern formation processes on a slow time scale, a conventional video camera providing a maximum frame rate of 25 frames per second (fps) and an exposure time of 40 ms is employed. In order to resolve the dynamics of patterns on a shorter time scale, the fast intensified camera "Proxitronic 1000 FPS," which allows an exposure time down to 5 ns with frame rates up to 1000 fps, is used.

Our observations show that the temperature of the cell influences the pattern formation processes and the behavior of patterns in the gas discharge. Therefore, the experimental setup has a tool to measure and control the temperature: One of the electrodes of the gas-discharge cell is placed on the finger of a cryogenic cooler whose temperature can be controlled via the flow of cold vapor from a vessel containing liquid nitrogen. The flow is controlled by a proportional-integrodifferential controller. The temperature is measured with a platinum "Pt-100" thermistor placed near the discharge cell. This system allows us to study pattern formation phenomena in the experimental cell in the temperature range from 100 K to 300 K.

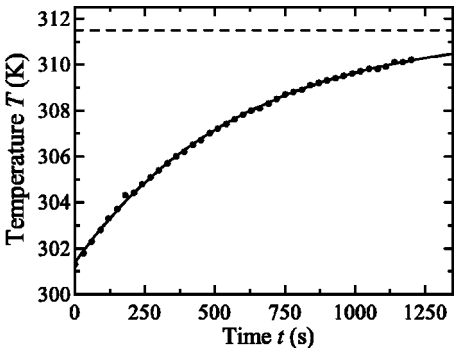

FIG. 2. Temperature in the nonthermostabilized cell. The dots indicate experimentally measured values of the cell temperature and the solid line is an exponential fit. The dashed line corresponds to the saturation value of the cell temperature $T_s=311.5$ K. Geometry of the system: Four circular discharge regions with diameters of 20, 15, 10, and 6 mm. The experiment was carried out in helium for $p=150$ hPa, $f=200$ kHz, and $\hat{U}=430$ V.

B. Cell heating

One of the reasons for the cell heating measurements is a very fragile behavior of some gas-discharge phenomena. A number of previous observations [32] indicate the existence of some intrinsic quantity, whose value is changing with time. For example, time-dependent changes in the behavior of current filaments have been observed on the time scale of some minutes.

The most probable candidate for this "hidden parameter" is the temperature of the cell. The analysis of the active discharge current and the voltage drop over discharge shows that the mean power dissipated in the cell is of order of 3 W. To check if this leads to substantial growth of the cell temperature, the temperature evolution during tens of minutes after switching on the device has been measured. For this experiment, the system has been prepared to be in the state of the homogeneous discharge, and the temporal dependence of the temperature in the cell has been measured in the absence of active stabilization. The result is depicted in Fig. 2. It can be seen that the temperature increases approximately by 10 K achieving the stationary state in 20 min. The plotted exponential fit gives the equilibrium temperature T_s

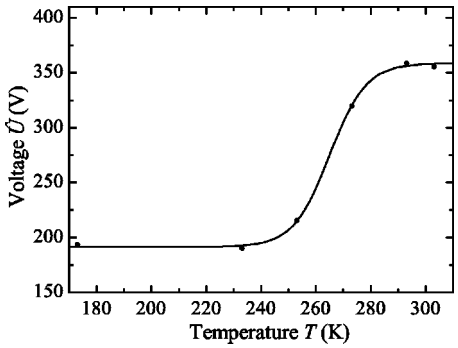

FIG. 3. Temperature dependence of the breakdown voltage in a ac gas-discharge cell. Geometry of the system: Experiment was carried out in helium by $p=298$ hPa He and $f=200$ kHz.

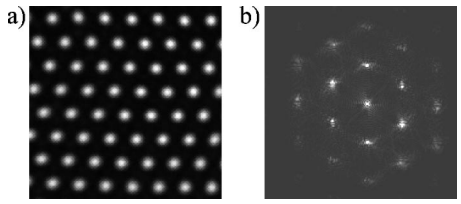

FIG. 4. Stationary hexagonal arrangement of filaments: Luminosity distribution (a) and corresponding Fourier image (b). The size of the depicted discharge area fragment is 1×1 cm. The overall active area is a single circular discharge domain of diameter $D=40$ mm. Parameters of the gas discharge: $p=305$ hPa He, $f=220$ kHz, $\hat{U}=380$ V, and $T=300$ K. Exposure time of the image $t_{\mathrm{exp}}=40$ ms.

≈ 311.5 K. If, in contrast, a thermal stabilization is used, the temperature stays permanently constant within 1 K in spite of the relatively high power dissipation in the system.

Obviously, the cell temperature is significant for pattern formation processes in the barrier discharge. The overheating of order of tens of kelvins may change the discharge properties dramatically. For the frequency range of at least $f\sim 0.1-1.0$ MHz, the mean dissipated power is proportional to the driver frequency. The experiments with driver frequencies of $f\sim 500$ kHz and above show that the glass electrodes could even be destroyed due to the inhomogeneity of either cell heating or heat sinking through the electrodes. The mechanical tension due to the temperature gradients in glass results in cracking or splintering after a few seconds of operation.

Our experimental observations show that the breakdown voltage depends on the cell temperature, as is shown in Fig. 3. This is a nontrivial dependence, where the breakdown voltage increases almost twice within a rather narrow temperature interval, while it remains almost constant outside this interval. Temperature dependence of the current–voltage characteristics has also been reported by other authors for a commercial glow discharge mass spectroscopic system [33]. The explanation of this dependence is beyond the scope of this paper.

The discharge properties depend on the cell temperature, which, in its turn, is influenced by the discharge. Thus, the state of the system may change in a nonthermostabilized cell (because of the self-heating of the discharge), although the experimental control parameters remain unchanged. Therefore, all of the following observations have been made with a stabilized temperature.

III. ROTATING HEXAGONAL PATTERNS

A. Patterns in the discharge system

For different parameters of the ac gas-discharge system, diverse patterns can be observed, e.g., single current filaments with radial symmetry [34], interacting pairs and clusters of filaments [35], bright domains [36], or concentric-ring patterns [37]. In this article, we concentrate on a complex type of pattern, which is made up of several interacting filaments: A 2D rotating hexagonal arrangement of localized current filaments. The rotating hexagonal pattern originates from a stationary hexagonal pattern, which consists of current filaments arranged on a 2D hexagonal grid. An example of the latter pattern is shown in Fig. 4(a) and the corresponding Fourier image is presented in Fig. 4(b). The filaments forming the hexagonal grid have a diameter in the order of 1 mm and fill the whole discharge area.

Under appropriate change of experimental conditions, the stationary hexagonal pattern starts rotating. This transition can also take place via a jerking of the pattern or via irregular translations along its "crystal axes." At elevated pressure, the rotating hexagonal pattern emerges directly from the homogeneous discharge. The transition scenarios may differ for different gases and for different values of system parameters.

The angular velocity of the rotation is rather high and does not allow the observation of the phenomenon with the naked eye or with a conventional CCD camera. In fact, the latter shows a radially symmetric luminosity distribution of the discharge with irregular luminosity change along the radius. The "Proxitronic 1000 FPS" intensified camera was used in order to provide the required time resolution. The rotation direction seems to be selected randomly and the angular velocities for both directions are equal. The pattern can also change the rotation direction spontaneously.

B. Changes in the electrical characteristics of the gas discharge

The transition from the stationary pattern to the rotating hexagonal pattern is also accompanied by a change of char-

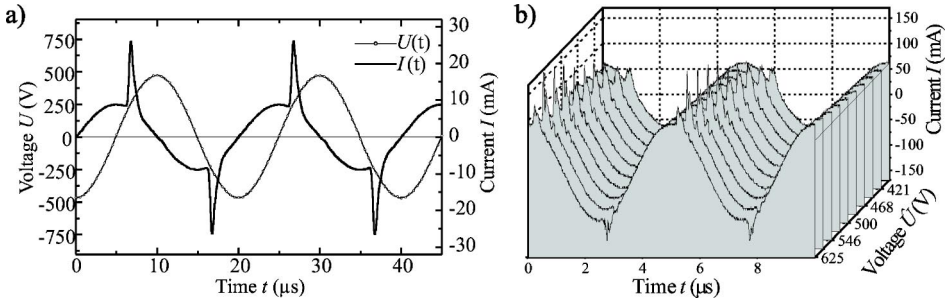

FIG. 5. (a) Schematic plot of the time evolution of the external voltage and the cell current in the planar ac gas-discharge system. (b) Dependency of the temporal evolution of the cell current on the driving voltage. The rear nine graphs ($\hat{U}=414-578$ V) correspond to a quasihomogeneous state and the front graph ($\hat{U}=625$ V) corresponds to rotating hexagonal state. The discharge cell contains four circular discharge regions with diameters $D_i=20$, 15, 10, and 6 mm. Parameters: $p=200$ hPa Ar, $f=200$ kHz, $\hat{U}=414-625$ V, and $T=273$ K.

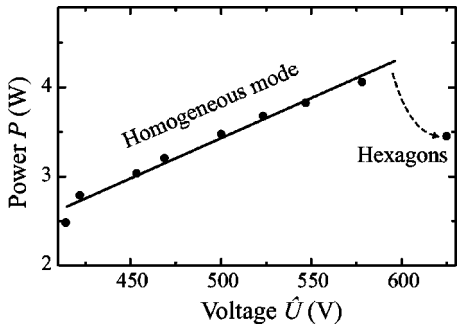

FIG. 6. Power dissipation during the transition to the rotating hexagonal state. The discharge cell contains four circular discharge regions with diameters D_i=20, 15, 10, and 6 mm. Parameters: p =200 hPa Ar, f=200 kHz, $\hat{U}$=414–625 V, and T=273 K.

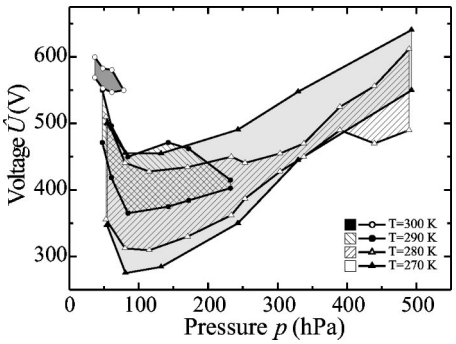

FIG. 7. Regions of existence of the rotating hexagonal pattern for different temperatures in helium. The region of existence for each temperature is outlined with a different hatching or shading to make the regions more distinguishable. Geometry of the system: Circular discharge domain with diameter D_1=20 mm; f=200 kHz.

acteristics of the gas discharge. Among them are the current and the power dissipated in the discharge. Generally, the displacement current in the discharge cell exhibits an oscillatory behavior similar to the external voltage and is phase shifted to the latter by $\varphi \approx \pi/2$.

When the voltage in the cell exceeds the ignition voltage, a large current can flow for a short time, resulting in a steep peak in the cell current, referred to as an active current [Fig. 5(a)]. This short pulse can also be observed in the current dynamics of the argon discharge recorded for different values of the amplitude of the externally applied voltage [Fig. 5(b)]. The amplitude of the displacement current for the ignition voltage at which the discharge is homogeneous ($\hat{U} \approx 421$ V) is marked by a thin horizontal line on the right side of the graph. It can be seen that the increments of both the idle and the active current are proportional to the voltage growth. Furthermore, the active current pulses are shifted to earlier moments with increasing voltage, because the ignition voltage in each oscillation is reached for smaller values of the phase if the amplitude of the voltage is greater [compare Fig. 5(a)]. The maximum voltage value ($\hat{U}$=625 V), corresponding to the rotating hexagonal state, also has a shift relative to the previous graph where the discharge is still homogeneous, but the amplitude of the active current is smaller.

Similar to the cell current, the power dissipation in the cell changes with the applied voltage. The course of the average power dissipation, starting from the ignition voltage of the discharge and ending with the voltage necessary for the development of a rotating hexagonal grid, is shown in Fig. 6. The power first grows linearly with an increase of the voltage, starting from 2.5 W at $\hat{U}$=414 V and reaches 4.1 W at $\hat{U}$=578 V. After the transition to the rotating hexagon, its value drops to 3.4 W. Such behavior is characteristic for transitions to both stationary and rotating hexagonal patterns.

C. Regions of existence

Here, we present regions in parameter space where the rotating hexagonal pattern exists. Figure 7 shows the regions of existence in the $(p, \hat{U})$ space for the pattern in helium for different temperatures. The largest interval of pressure and voltage where rotation occurs was observed for the temperature T=270 K. This region remains practically unchanged down to $T \sim 260$ K. At a lower temperature, the discharge undergoes a transition to a homogeneous mode, for which the optical radiation spectrum differs strongly from the one observed at room temperature, and no structures can be observed.

With increasing temperature, the region of existence contracts as can be seen in Fig. 7 for T=280–300 K. Moreover, we could not find rotating hexagonal structure for $T>300$ K. This clarifies why no rotating hexagonal patterns can be observed without temperature control: The power dissipated in the cell increases the gas temperature to $T>300$ K. The power, dissipated in the cell after the transition to the structured discharge with hexagonal arrangement of filaments, remains in the order of some watts. Only permanent temperature control may assure the stability of the system position in the parameter space and, consequently, the reproducibility of the experimental results. Thus, the rotating hexagonal pattern emphasizes the crucial importance of cell temperature for pattern formation in barrier gas discharge.

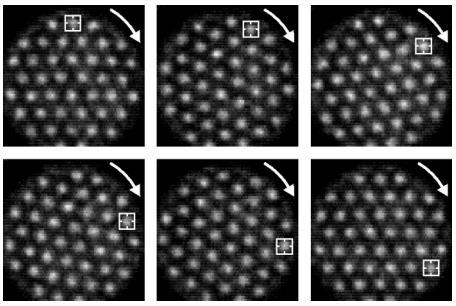

FIG. 8. Image sequence of rotating hexagonal filament arrangement. The arrows indicate the rotation direction and the cursor traces a selected filament. The active area is a circular discharge region with diameter D=15 mm. Parameters are: p=113 hPa He, f=200 kHz, $\hat{U}$=400 V, and T=280 K. The time interval between images is Δt=32 ms, exposure time of each frame t_{exp}=100 μs.

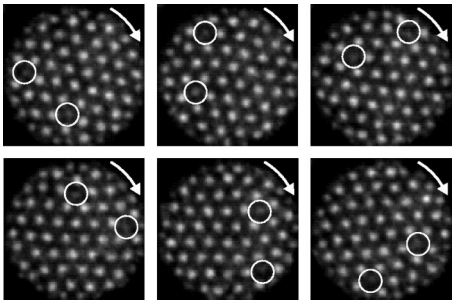

FIG. 9. Image sequence of a rotating hexagonal filament arrangement with embedded structural defects. The defects are marked with white circles. The arrows indicate the rotation direction. The active area is a circular discharge region with diameter $D=15$ mm. Parameters are: $p=163$ hPa He, $f=200$ kHz, $\hat{U}=372$ V, and $T=280$ K. The time interval between images is $\Delta t=32$ ms, exposure time of each frame $t_{\mathrm{exp}}=100$ μs.

D. Interaction of the filaments

The interaction between the filaments forming the structure is strong enough so that the whole structure rotates as a rigid body (see the image sequence in Fig. 8) and rearrangements of the filaments are rare. One of the filaments in Fig. 8 is marked by a cursor and its position is traced through all images. From the movement of the filament, one can see that the structure rotated by an angle of 120° within 160 ms and is mapped into itself due to the symmetry of the structure.

Furthermore, if point defects are present in the grid or arise in the course of a rearrangement, they rotate together with the structure. This situation is illustrated by the image sequence in Fig. 9, which was recorded over 160 ms. The rotation direction is marked by white arrows in the upper right corner of each image. One of the defects is located near the boundary of the structure whereas the other one is further inside the filamentary grid. Note, that the defects cause only local rearrangements in the structure. Structure defects may strongly influence the angular velocity of the pattern. For instance, for the hexagon with defects shown in Fig. 9 the rotation by an angle of approximately 280° takes the same time as the rotation by 120° for the regular pattern. The angular velocity depends also on the diameter of the discharge domain. More peculiarities of the rotation of the pattern will be discussed in Sec. III E.

It can be observed that the spatial period length of the structure, i.e., the distance between two neighboring filaments along one of the main axes of the hexagon, changes with the cell voltage. The dependence of the spatial period length on the driving voltage is presented in Fig. 10(a). As the total discharge current increases with the voltage and the current pro each filament remains unchanged, the number of filaments in the active area increases with the applied voltage. Thus, the density of the grid grows, resulting in a strong decrease of the period length λ.

Figure 10(b) shows the light emission profiles of two neighboring filaments for an external voltage of $\hat{U}=436$ V, corresponding to the minimum observed period length. The experimental profile (dots) is fitted with two Gaussian curves (solid lines), which illustrate the result that would be obtained from two isolated filaments. In addition, the sum of the single fits is depicted as a dashed line. Figure 10(b) shows that the pattern modulation depth is approximately 50%. A further approach of the filaments would result in a joining of them, which would probably destroy the integrity of the single filaments. Indeed, an experimental examination confirms that the pattern can no longer exist if the voltage is further increased.

The interaction between the filaments in the hexagonal pattern may have diverse characters. It may be clearly repulsive, if the discharge area is considered as a potential well, analog to 2D coulomb crystals which exhibit a similar dynamics (see [27,28]). It is also possible, that repulsive and attractive interaction may alternate with the distance between the filaments. Here, filaments may lock in on stable fixed points where the repulsive interaction changes to attractive interaction. Thus, the question about the interaction kind and its mechanism is still open and is a subject of further investigation.

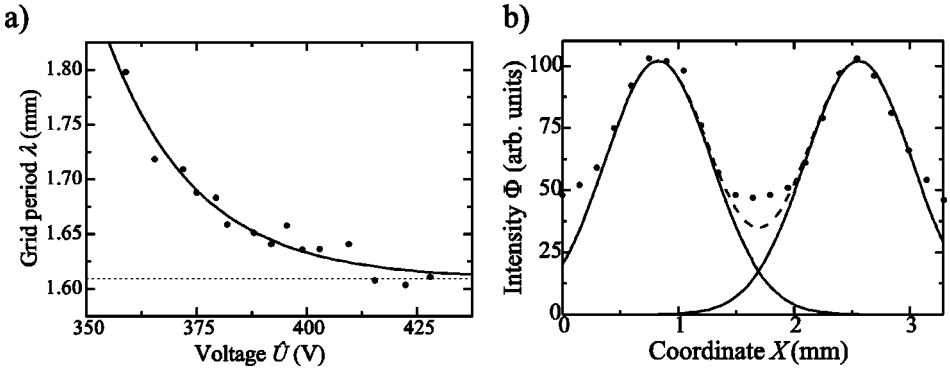

FIG. 10. (a) Spatial period length of the rotating hexagonal grid as a function of the applied voltage. The experimental values are plotted as dots and the solid line represents an exponential fit to the experimental data points. The dashed line marks the limit value $\lambda \approx 1.61$ mm. The active area is a circular discharge region with diameter $D=20$ mm. (b) Experimentally recorded luminance density profiles (black dots) of two neighboring filaments at the maximum voltage $\hat{U}=436$ V. The single profiles were fitted with Gaussian distributions (solid lines), in addition, the sum of the fit curves is depicted (dashed line). Parameters: $p=163$ hPa He, $f=200$ kHz, $\hat{U}=350-430$ V, and $T=280$ K.

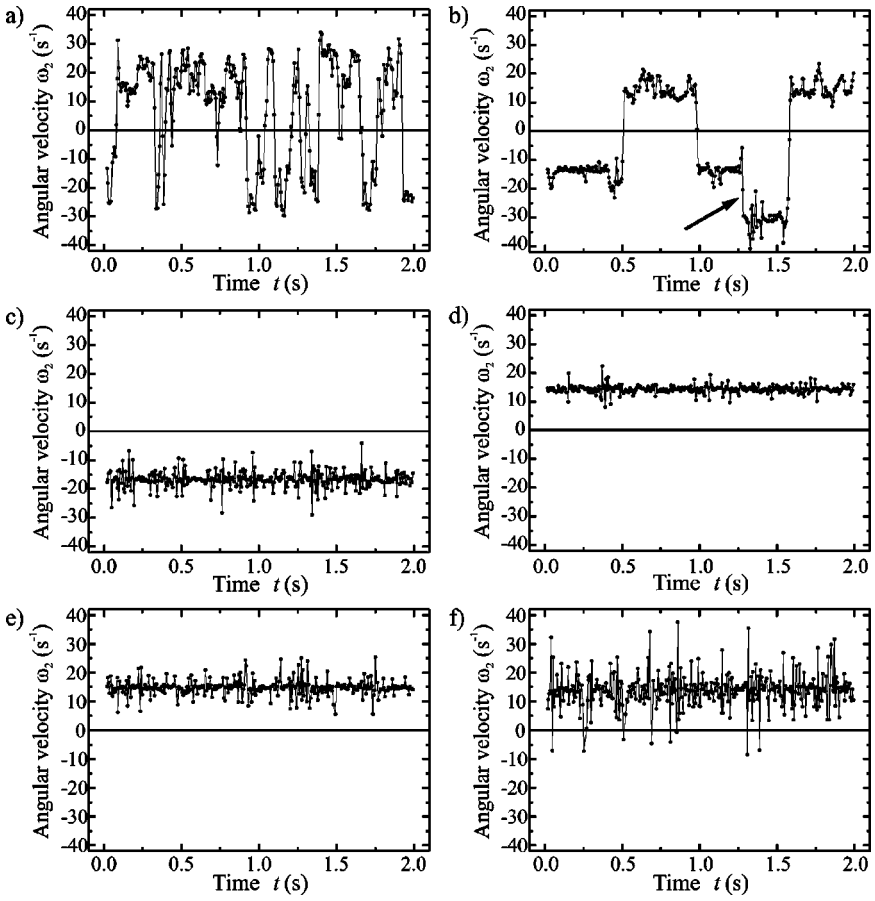

FIG. 11. Angular velocity of the rotating hexagonal structure as a function of time. The diameter of the discharge area is $D_2=15$ mm. Parameters: $f=200$ kHz, $p=163$ hPa He, and $T=280$ K. Voltage: (a) $\hat{U}=365$ V; (b) $\hat{U}=372$ V; (c) $\hat{U}=375$ V; (d) $\hat{U}=382$ V; (e) $\hat{U}=403$ V; and (f) $\hat{U}=428$ V.

E. Properties of the rotational motion

In order to analyze the dynamics of the pattern, angular velocity measurements have been carried out in the thermostabilized cell with four circular discharge domains of different diameter separated by means of a spacer with corresponding geometry. All domains are placed in the same gas vessel, have common electrodes and are fed with the same supply voltage. The angular velocity of hexagonal structures in all domains has qualitatively the same dynamics, which depends on the cell voltage. Characteristic cases are presented in Fig. 11.

In Fig. 11(a), the velocity plot looks irregular with a permanent change of the rotation direction, making it hard to determine a dominant value of the velocity. The presented behavior is observed close to the lowest voltage limit where the rotating pattern exists. An increase of the voltage leads to the situation depicted in Fig. 11(b), in which the motion becomes more regular. The situation is characterized by rather long periods with nearly constant angular velocity and short transition periods in which the rotation changes its direction. One more remarkable peculiarity of this plot is the jump of the average rotation velocity, marked in the plot with an arrow. The velocity jump in the case of $\hat{U}=372$ V seems to be due to a disturbance of the hexagonal structure (see Fig. 12). The moments in which defects emerge and disappear coincide with the moments in which the velocity jump starts and stops.

If the voltage is further increased, the rotation becomes even more stable, so that changes in the direction of motion practically no longer occur and the deviation from the average velocity decreases [Figs. 11(c) and 11(d)]. The deviation reincreases if the increase of the voltage is continued, although changes in the direction of the motion are no longer observed [Figs. 11(e) and 11(f)].

Another interesting aspect is the influence of the size of the active domain on the velocity of the rotation. To investigate this matter, the average angular velocity was measured on two domains of different sizes: $D_1=20$ mm and $D_2=15$ mm for varying values of the applied voltage (Fig. 13). As, according to the experimental observations, the hexagonal structure has no preferred rotation direction, only the absolute values of the angular velocity are considered. One can see that the mean values of the angular velocity ω_1 for the larger domain D_1 are almost voltage independent. The

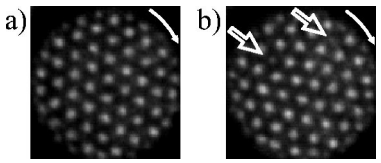

FIG. 12. Point defects and rotation velocity doubling for the situation corresponding to the Fig. 11(b). (a) Pattern at the moment $t=1218$ ms, i.e., before the rotation frequency was doubled, and (b) at $t=1408$ ms, i.e., after the frequency doubling. The white curved arrows show the rotation direction and the contoured arrows in (b) mark the structural defects in the fast rotating pattern. The diameter of the discharge domain is $D_2=15$ mm. Parameters are: $p=163$ hPa He, $f=200$ kHz, $\hat{U}=372$ V, and $T=280$ K.

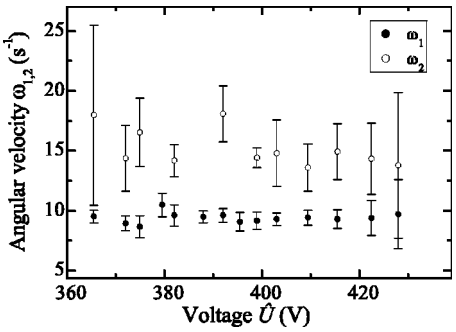

FIG. 13. Absolute value of the pattern angular velocity as a function of the driving voltage for two circular domains (D_1 = 20 mm, and D_2 = 15 mm). Values of ω_1 and ω_2 are marked with filled and open circles, respectively. Parameters are: p = 163 hPa He, f = 200 kHz, $\hat{U}$ = 350–430 V, and T = 280 K.

rotation in the larger domain D_1 is more stable and the standard deviations for measured velocities are also relatively small. The angular velocities ω_2 for the small domain D_2 are higher than ω_1 at the same parameters. The stability of the rotation is lower, so that the standard deviation of ω_2 for a constant voltage is higher. Outer filaments of the structure have a maximal linear velocity of about 10 cm/s. We note that this velocity is the same for all domains for given control parameters and does not markedly depend on the gas pressure. This maximal velocity of a filament clarifies the reciprocal dependance of the angular velocity of the hexagonal pattern on the radius of the discharge domain.

The stability of the rotation depends on the applied voltage. This can be seen also in Fig. 11: The standard deviation of the angular velocity is extremely high for the lowest measured voltage $\hat{U}$ = 365 V [Fig. 11(a)], where the rotation is fragmentary and its direction changes permanently. Toward the middle of the voltage region, the standard deviation drops and is minimal for $\hat{U}$ = 382 V [Fig. 11(d)]. Approaching the upper limit of the existence region of the pattern the stability of the rotation decreases again and is minimal for the highest voltage $\hat{U}$ = 428 V [Fig. 11(f)].

The perturbation intensity increases with both increased and decreased voltage from the center of the existence region. One of possible reasons for this effect can be more frequently emerging structure defects, which strongly influence the rotation process [see Figs. 11(b) and 12].

F. Symmetry breaking

When analyzing the geometry of stationary hexagonal patterns, one always finds nearly perfect symmetry of the cluster. For an onset of rotation, the symmetry must be broken [38]. The breaking of the symmetry can be observed in the experimental system, where the rotating patterns exhibit a slight asymmetry with respect to the direction of rotation. The filaments are slightly shifted from the positions corresponding to the ideal hexagonal grid. This shift is normally less than the visible diameter of the filament. Thus, it cannot be measured without a software procession of the experimental data. In the simplest way, the deformation grade of the pattern can be characterized by a quantity M, which is referred to as *lag momentum*. Figure 14 illustrates the definition of the lag momentum.

The "ideal grid" of a stationary hexagonal arrangement of filaments is shown schematically in Fig. 14(a). Gray filled circles represent filaments, and solid lines are the main axes of the structure. At the onset of rotation, the structure will be distorted, leading to a deformation as shown in Fig. 14(b). The filaments are shifted by a certain angle from their initial positions, which depends on the distance from the center of the structure. The lag momentum of the structure is then defined by the formula

$$\mathbf{M} = \frac{1}{n-7}\sum_{i=8}^{n}\frac{\mathbf{r}_i \times \boldsymbol{\delta}_i}{|\mathbf{r}_i|}, \tag{1}$$

where n is the total number of filaments in the gas discharge, $\mathbf{r}_i$ is the radius vector of ith filament (the origin is located at the center of the structure) and $\boldsymbol{\delta}_i$ is the lag vector of the filament, characterizing the shift of the filament from its position in the geometrically perfect hexagonal grid. The ideal grid orientation in the calculation of the lag momentum is determined by the seven filaments nearest to the center of rotation. Hence, their lag momentum is minimized by aligning the ideal hexagonal matrix with them, so that they do not have to be considered in the calculation.

For the example presented in Fig. 14(c), M is positive. In the drawing are shown only seven central filaments used for the grid orientation and the filaments at the corners of the distorted rotating structure. They are connected by solid lines which mark the outer boundary of the structure and by deformed main axes l_1', l_2', l_3'. The contour of the ideal hexagonal structure is aligned to the central filaments; the corresponding main axes l_1, l_2, and l_3 as well as the ideal positions for the filaments at the corners are depicted using dashed-dotted lines. The ideal position of the filament on the right side of the axis l_1 is denoted by $\mathbf{r}_i$, and the shift to its actual position is denoted by $\boldsymbol{\delta}_i$. The resulting lag momentum of the filament $\mathbf{M}_i$, defined as the vector product of the radius vector and of the shift normalized to $|\mathbf{r}_i|$, is shown as a gray

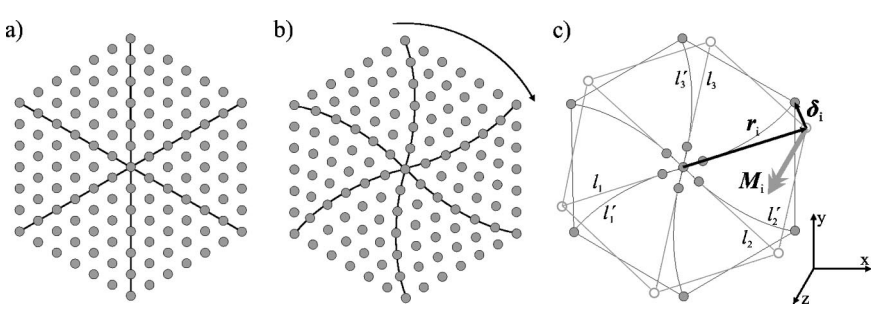

FIG. 14. Definition of the lag momentum. (a) Arrangement of the filaments in the case of stationary hexagonal pattern, (b) structural distortion in the case of rotation, and (c) illustration for the calculation of the lag momentum.

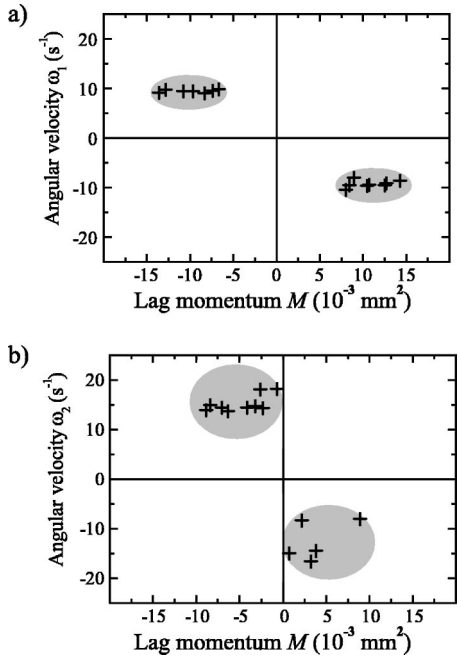

FIG. 15. Angular velocity versus lag momentum for the discharge domains $D_1=20$ mm (a) and $D_2=15$ mm (b). Each cross represents a measurement averaged over 2000 frames, of both lag momentum and angular velocity. Parameters: $p=163$ hPa He, $f=200$ kHz, $\hat{U}=350-430$ V, and $T=280$ K.

arrow with a doubled spike. It is directed along the z axis of the coordinate system shown in the right bottom of Fig. 14(c).

The deformation of the structure leads to the symmetry breaking of the highly symmetric C_{6v} hexagonal arrangement. Only the rotational symmetry C_6 stays preserved. The sign of the lag momentum is well defined by the rotation direction. There seems to be no correlation between the values of angular velocity and of the lag momentum for different voltages (Fig. 15). Moreover, the angular velocity of hexagons seems to be voltage independent (see Fig. 13). A strong dependence of the angular velocity on the size of the hexagonal domain has been observed. The rotation on larger domains is obviously slower than on smaller ones. This fact can be explained if we assume well-defined maximal speed of a single filament.

IV. CONCLUSION

The experimental observation of a rotating hexagonal pattern on constricted circular domains has been reported. The transition from the stationary hexagonal pattern to the rotating hexagonal pattern is accompanied by a lowering of the pattern symmetry. The dissipated power and the shape of the active current spike change as well. We have demonstrated that, in the investigated case, the thermal stabilization of the system is necessary for the observation of the rotating hexagonal pattern.

It has been shown that the average angular velocity of the pattern is almost voltage independent and is determined by the dimension of the discharge domain. The angular velocity decreases with an increase of the domain radius. It should be stressed that the maximal linear velocity of outer filaments seems to be the same for all domains tested. It also does not depend on the gas pressure. The appearance of structural defects can result in a notable change of the rotation velocity. This fact may be helpful for the explanation of the physical background of such a collective motion phenomenon in barrier discharge.

ACKNOWLEDGMENTS

The authors thank Dr. Shalva Amiranashvili for fruitful discussions and the Deutsche Forschungsgemeinschaft (DFG) for the financial support.

[1] M. C. Cross and P. C. Hohenberg, Rev. Mod. Phys. **65**, 851 (1993).
[2] A. V. Gorbatyuk and I. E. Panaiotti, Tech. Phys. Lett. **29**, 370 (2003).
[3] A. V. Gorbatyuk and F.-J. Niedernostheide, Phys. Rev. B **59**, 13 157 (1999).
[4] F.-J. Niedernostheide, H. J. Schulze, O. Freyd, M. Bode, and A. V. Gorbatyuk, Chaos, Solitons Fractals **17**, 255 (2003).
[5] B. G. Bosch and R. W. H. Engelmann, *Gunn-Effect Electronics* (Pitman, London, 1975).
[6] S. Facsko, T. Dekorsy, C. Koerdt, C. Trappe, H. Kurz, A. Vogt, and H. L. Hartnagel, Science **285**, 1551 (1999).
[7] A. A. Golovin, S. H. Davis, and P. W. Voorhees, Phys. Rev. E **68**, 056203 (2003).
[8] H. M. Jaeger, S. R. Nagel, and R. P. Behringer, Rev. Mod. Phys. **68**, 1259 (1996).
[9] J. A. Drahun and J. Bridgewater, Powder Technol. **36**, 39 (1983).
[10] K. M. Hill, J. F. Gilchrist, J. M. Ottino, D. V. Khakhar, and J. J. McCarthy, Int. J. Bifurcation Chaos Appl. Sci. Eng. **9**, 1467 (1999).
[11] A. Adamatzky, *Computing in Nonlinear Media and Automata Collectives* (IOP, Bristol, 2001).
[12] D. Z. Anderson and J. Feinberg, IEEE J. Quantum Electron. **25**, 635 (1989).
[13] M. Sedlatscek, T. Rauch, C. Denz, and T. Tschudi, Opt. Mater. (Amsterdam, Neth.) **4**, 376 (1995).
[14] D. Statman and J. C. Lombardi, J. Nonlinear Opt. Phys. Mater. **7**, 47 (1998).
[15] A. L. Hodgkin and A. F. Huxley, J. Physiol. (London) **117**, 500 (1952).
[16] R. A. Gray, J. Jalife, A. V. Panfilov, W. T. Baxter, C. Cabo, J. M. Davidenko, A. M. Pertsov, P. Hogeweg, and A. T. Winfree, Science **270**, 1222 (1995).
[17] R. Friedrich and C. Uhl, Physica D **98**, 171 (1996).
[18] J. D. Murray, *Mathematical Biology* (Springer, Berlin, 1993).

[19] Y. A. Astrov, L. M. Portsel, S. P. Teperick, H. Willebrand, and H.-G. Purwins, J. Appl. Phys. **740**, 2159 (1993).
[20] R. Friedrich, G. Radons, T. Ditzinger, and A. Henning, Phys. Rev. Lett. **85**, 4884 (2000).
[21] B. S. Kerner, Phys. Rev. Lett. **81**, 3797 (1998).
[22] F. H. Busse, J. Fluid Mech. **30**, 625 (1967).
[23] P. K. Maini, K. J. Painter, and N. P. Chau, J. Chem. Soc., Faraday Trans. **93**, 3601 (1997).
[24] A. de Wit, Adv. Chem. Phys. **109**, 435 (1999).
[25] Q. Ouyang and H. L. Swinney, Nature (London) **352**, 610 (1991).
[26] F. Melo, P. B. Umbanhowar, and H. L. Swinney, Phys. Rev. Lett. **75**, 3838 (1995).
[27] V. A. Schweigert and F. M. Peeters, Phys. Rev. B **51**, 7700 (1995).
[28] A. Melzer, M. Klindworth, and A. Piel, Phys. Rev. Lett. **87**, 115002 (2001).
[29] Y. A. Astrov and Y. A. Logvin, Phys. Rev. Lett. **79**, 2983 (1997).
[30] E. Ammelt, Y. A. Astrov, and H.-G. Purwins, Phys. Rev. E **58**, 7109 (1998).
[31] I. Brauer, E. Ammelt, and H.-G. Purwins, Proceedings of the 24th International Conference on Phenomena in Ionized Gases (ICPIG), Centre de Phys. Plasmas et leurs Applications de Toulouse, Toulouse, France, 1999, pp. 141–142.
[32] I. Brauer, Ph.D. thesis, WWU Münster, 2000.
[33] M. Kasik, C. Michellon, and L. C. Pitchford, J. Anal. At. Spectrom. **17**, 1398 (2002).
[34] H. Willebrand, F.-J. Niedernostheide, E. Ammelt, R. Dohmen, and H.-G. Purwins, Phys. Lett. A **153**, 437 (1991).
[35] I. Müller, E. Ammelt, and H.-G. Purwins, International Conference on Phenoma in Ionized Gases ICPIG XXIII, Institute of Plasma Physics and Laser Microfusion (IPPLM), Warsaw, Poland, 1997, Vol. II-182–II-183.
[36] E. Ammelt, D. Schweng, and H.-G. Purwins, Phys. Lett. A **179**, 348 (1993).
[37] E. L. Gurevich, A. L. Zanin, A. S. Moskalenko, and H.-G. Purwins, Phys. Rev. Lett. **91**, 154501 (2003).
[38] A. S. Moskalenko, A. W. Liehr, and H.-G. Purwins, Europhys. Lett. **63**, 361 (2003).